Configurable Microwave Filter for Signal Processing Based on Arrays of Bistable Magnetic Nanowires

Rossana Ramírez-Villegas, Isabelle Huynen, *Senior Member, IEEE*, Luc Piraux, Armando Encinas, and Joaquin De La Torre Medina

Abstract—Using arrays of bistable magnetic nanowires, we show that their microwave absorption properties can be reversibly configured using low magnetic field cycling by virtue of the double ferromagnetic resonance absorption spectra. These characteristics lead to a single bifunction microwave filter that can be configured to work as a bandstop or a bandpass filter, making these materials very attractive for compact multifunction planar microwave devices. The bifunction microwave properties of these systems are successfully predicted using a mean field model for their magnetic configuration-dependent effective permeability.

Index Terms—Heterostructure device physics, magnetic materials, microwave filters, multifuctional systems, multimode filters, nanostructures.

I. INTRODUCTION

WITH the growing demand for consumer-oriented wireless communication systems, there is an increasing need and interest for the development of new materials that can potentially be exploited for planar devices capable of performing microwave signal processing [1], [2]. Microwave devices based on low-dimensional ferromagnetic structures such as thin films, multilayers, and nanoparticle arrays have attracted a lot of attention. This is motivated because they provide higher operation frequencies than conventional ferrites and their absorption characteristics can be fine-tuned by adjusting their magnetic properties [3]–[5]. Particularly, arrays of nanowires (NWs) have been exploited for the fabrication of unbiased and field configurable microwave isolators [6], [7], circulators [8], [9], phase shifters [10], [11], and noise suppresors [12]. Recently, the concept of field configurable microwave devices has been brought forward. This is as an alternative approach based on bistable magnetic particles, which have the potential of allowing reconfiguration of its magnetic and microwave absorption properties using field cycling [13]–[15]. Microwave filters are among the most important signal processing elements [16], [17] and the four types of filters, bandstop, bandpass, low-pass, and high-pass, are required either alone or combined. This opens the path to seek for multifunction behavior using a single material, contrary to the usual approach of having a single function material. Previous bandpass filter modules were commonly designed by employing a pair of cascaded elements like two different filters [18], resonators [19]–[22], and bandstop filters based on either meandered-like lines [23], or two different magnetic materials [3]. In most cases, these modules operate at frequencies from L-band to X-band and their multifunctional microwave characteristics consist in tuning the passband center frequency and bandwidth. Simultaneous functionalities of bandpass and bandstop filters at X-band have been achieved in magnetic field tunable modules composed of cascaded passive microstrip composites and inductive elements of a stepped impedance low-pass filter [24].

Here, we discuss the applicability of the double ferromagnetic resonance (FMR) effect for the conception of a bifunction and low-field cycling microwave filter based on arrays of bistable NWs. In particular, we show that these systems can perform as a bandpass filter due to the double FMR effect observed in unsaturated states and as a bandstop filter when the system is at remanence. The reversible passage between both the filter modes is achieved upon magnetic configuration in stable magnetic states and their microwave characteristics can be engineered by choosing appropriate material parameters such as the packing fraction and the coercive field of the NW array. The advantages of our module as a promising substrate for RF integrated devices are its low power consumption, good thermal stability, and its simple and compact design as a lightweight planar structure. As discussed in Section II, the proposed device consists of a short and straight microstrip line on a nanocomposite containing NWs of a single magnetic material. In Section III, we propose an analytical mean field model for the configuration-dependent effective permeability, which allows predicting the FMR absorption spectra and then the characteristics of our multifunction microwave filter based on arrays of bistable magnetic NWs. Moreover, in Section IV, we show that the present device is capable of working in two different filtering modes and has passband bandwidths and operation frequencies in the respective ranges

TABLE I

EXPERIMENTAL VALUES FOR THE SATURATION MAGNETIZATION (M_s), PACKING FRACTION (P), AND GYROMAGNETIC RATIO (γ) FOR THE ARRAYS OF NWS CONSIDERED IN THIS PAPER

Material	M_s (emu/cm^3)	P (%)	γ (GHz/kOe)
Ni$_x$Fe$_{100-x}$; $76 \leq x \leq 83$	$788 - 890$	$3.4 - 10$	2.97
Co$_y$Fe$_{100-y}$; $54 \leq x \leq 75$	$1721 - 1950$	$2.8 - 8.5$	$2.96 - 2.98$
Co	1400	$1.6 - 5.6$	3.05

of 5–18 and 7–32 GHz. Although the operation frequency of our module is fixed for a specific magnetic material, its major novelty is the reversible passage between the bandpass and bandstop filtering modes.

II. DEVICE TOPOLOGY AND FABRICATION

Arrays of 35-nm diameter Ni$_x$Fe$_{100-x}$, Co$_y$Fe$_{100-y}$ (with percentages $76 \leq x \leq 83$ and $54 \leq y \leq 75$), and fcc-like Co NWs without magnetocrystalline anisotropy contributions were considered. These were fabricated by electrodeposition into the pores of 21-μm thick track etched polycarbonate (PC) and 90-μm thick anodic aluminum oxide (AAO) porous membranes. The saturation magnetization (M_s), packing fraction (P), and gyromagnetic ratio (γ) for the NiFe, CoFe, and Co NWs are summarized in Table I. Electrodeposition of Co, NiFe, and CoFe NWs was carried out, respectively, at constant potentials of -0.95 V and in the range -0.9 to -1.2 V versus Ag/AgCl [25], [26]. Electrolytes of 238.48 gl^{-1} CoSO$_4$ + 30 gl^{-1} H$_3$BO$_3$ with pH = 2; 131.42 gl^{-1} NiSO$_4$ + 5.56 gl^{-1} FeSO$_4$ + 30 gl^{-1} H$_3$BO$_3$ with pH = 3.8; and 40 gl^{-1} FeSO$_4$ + 80 gl^{-1} CoSO$_4$ + 30 gl^{-1} H$_3$BO$_3$ were used for the growth of Co, NiFe, and CoFe NWs, respectively. Frequency swept FMR measurements were done using a 150-μm-wide microstrip line, which was evaporated on the free side of the membrane following electrodeposition. The schematic of the structure of the proposed prototype is shown in Fig. 1(a) and photographs of 2- and 0.7-cm-long real devices, based on PC and AAO porous membranes, are, respectively, shown in Fig. 1 (b) and (c). A photograph of the experimental setup, displaying the device-under-test (DUT) connected to the vector network analyzer (VNA) and within the poles of an electromagnet is shown in Fig. 1(d). The transmission coefficient between 0 and 45 GHz was recorded using a VNA, while a constant magnetic field (H) was applied parallel to the NWs [26]. Magnetometry measurements were performed using an alternating gradient magnetometer (AGM). All the measurements in this paper were done at room temperature.

III. PERMEABILITY MODEL FOR ARRAYS OF BISTABLE NWS

Arrays of bistable NWs present a double FMR absorption in unsaturated states, which is related to the fraction m_+ and m_- of NWs magnetized in the positive ($+$) and negative ($-$) directions along the NW-axis [26], [27]. The fraction of $m_\pm$ NWs is related to the magnetic state m of the whole array via the equation $m_\pm = (1 \pm m)/2$ and account for the amplitude of its corresponding absorption peak. The minima of
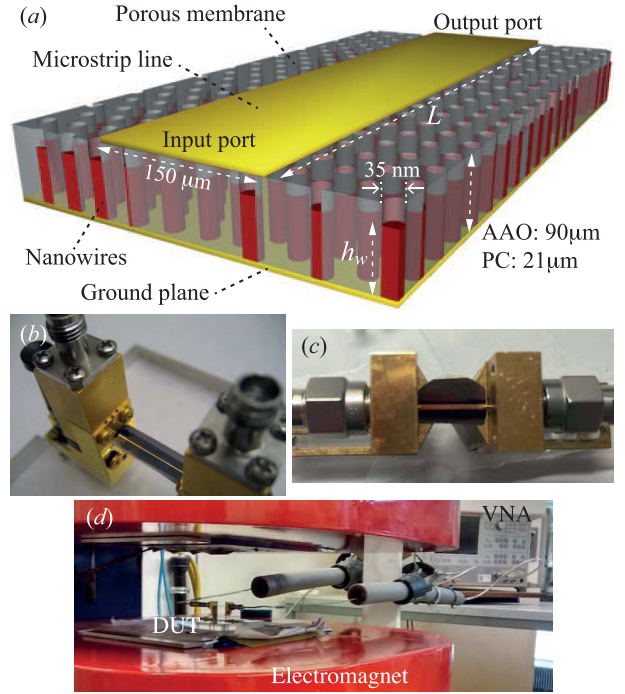
Fig. 1. (a) Schematics of the bifunction microwave filter structure based on an array of bistable magnetic NWs, showing the input and output ports. Photographs of two prototypes based on (b) PC and (c) AAO porous membranes with microstrip lines having respective lengths of 2 and 0.7 cm. (d) Photograph of the experimental setup, displaying the measurement equipment (VNA), the electromagnet, and the DUT.

these peaks are located at the $f_{m_\pm}$ resonance frequencies [26], which can be written as

$$f_{m_\pm} = f_{\text{bp}} \pm \frac{1}{2}\Delta f \qquad (1)$$

where

$$f_{\text{bp}} = \frac{1}{2}(f_{m_+} + f_{m_-}) = 2\pi M_s \gamma \left(1 - \frac{3}{2}P\right) \qquad (2)$$

is the configuration-independent frequency located at the midpoint between both $m_\pm$ FMR absorptions for which no attenuation takes place. Therefore, it defines the bandpass frequency for the bifunction microwave filter proposed herein, which will be discussed afterward. The term Δf in (1) corresponds to the frequency bandwidth given by the separation between the f_{m_+} and f_{m_-} resonance frequencies, that is,

$$\Delta f = f_{m_+} - f_{m_-} = 2\gamma(H - H_{\text{int}}) \qquad (3)$$

where H is the applied dc field and $H_{\text{int}} = 3\pi M_s P m$ is the configuration-dependent interaction field of the array of NWs [26]. As seen in (1), both f_{m_+} and f_{m_-} are obtained by either adding or subtracting one half the value of their separation to the midpoint frequency f_{bp}. In any case, Δf is such that it is negative for $H < 0$ and positive for $H > 0$. Besides, in the uniform precession mode the magnetization of each NW, considered as a macrospin, is driven by an applied RF magnetic field ($\vec{h}$) and obeys the Landau–Lifshitz–Gilbert equation of motion. Solving this equation leads to the ac permeability tensor ($\bar{\mu}$) that relates the total RF magnetization ($\vec{m}$) of the NWs with $\vec{h}$ through the equation $\vec{m} = \mu_0(\bar{\mu} - \bar{1})\vec{h}$. In this

sense, the permeability tensor of the array of NWs corresponds to the addition of the permeability tensors for the $m_\pm$ NWs, that is, $\bar{\mu} = \bar{\mu}_{m_+} + \bar{\mu}_{m_-}$, where $\bar{\mu}_{m_\pm}$ is the permeability tensor of the $m_\pm$ NWs population which reads as

$$\bar{\mu}_{m_\pm} = \begin{pmatrix} \mu_{m_\pm} & \mp j\kappa_{m_\pm} & 0 \\ \pm j\kappa_{m_\pm} & \mu_{m_\pm} & 0 \\ 0 & 0 & m_\pm \end{pmatrix} \qquad (4)$$

where

$$\mu_{m_\pm} = \frac{1}{2}(1 \pm m)\left[1 + \frac{Ph_w f_m(f_{m_\pm} + j\alpha f)}{(f_{m_\pm} + j\alpha f)^2 - f^2}\right] \qquad (5)$$

$$\kappa_{m_\pm} = \frac{1}{2}(1 \pm m)\left[\frac{Ph_w f(f_{m_\pm} + j\alpha f)}{(f_{m_\pm} + j\alpha f)^2 - f^2}\right]. \qquad (6)$$

In (5) and (6), h_w is the normalized length of the NWs obtained by dividing its length by the membrane thickness, $f_m = 4\pi M_s \gamma$, f is the RF-frequency, α is the damping factor, and $f_{m_\pm}$ is given by (1). Equations (5) and (6) allow to obtain the effective permeability of the array of NWs

$$\mu_{\text{eff}} = \frac{(\mu_{m_+} + \mu_{m_-})^2 - (\kappa_{m_+} - \kappa_{m_-})^2}{\mu_{m_+} + \mu_{m_-}}. \qquad (7)$$

Considering an exact match impedance of 50 Ω between the microstrip line and the VNA, the measured effective permeability (μ_{exp}) is obtained from the measured complex transmission factor (S_{exp}) using the expression

$$\sqrt{\mu_{\text{exp}}} = 1 + \frac{jc_0 \ln(S_{\text{exp}})}{2\pi f L \sqrt{\varepsilon_{\text{eff}}}}. \qquad (8)$$

In this equation, c_0 is the speed of light in vacuum, L is the length of the microstrip line, and ε_{eff} is the effective permittivity of the composite material [29], which depends on the bulk permittivity of PC (=2.89) and AAO (=9.8) membranes. Fig. 2(a) and (b) shows the calculated (dotted lines) and measured (continuous lines) real and imaginary parts of the effective permeability obtained using (7) and (8) for the array of Ni$_{83}$Fe$_{17}$ NWs embedded in a PC porous membrane with $P = 3.4\%$, $L = 2.2$ cm, and $h_w = 0.3$. As seen, very good agreement between the theoretical and measured curves recorded at different unsaturated states is observed. These states are configured magnetically under the application of different constant magnetic field values over the descent part of the hysteresis loop (see the inset). As the magnetic field is reversed from positive to negative saturation, the population of m_+ (m_-) NWs decreases (increases), resulting in a continuous decrease (increase) of the magnetic signature at low (high) frequencies in both the real and imaginary parts of the effective permeability. Stronger variations of the real part and larger amplitudes of the imaginary part of the permeability at the FMR absorption are associated with higher magnetic losses that increase with the number of NWs. The low values of both parts of the permeability observed for the diluted system in Fig. 2 result from both the low values of the packing fraction and NWs length. That is, increasing the volume of the magnetic material will lead to higher magnetic losses or larger FMR absorptions. The curves in Fig. 2 show that it is possible to configure the relative amplitude of both the peaks in the absorption spectra, which can be made asymmetrical by
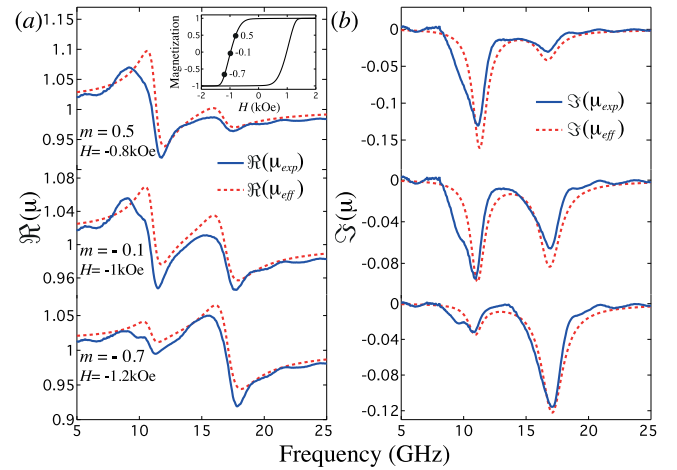
Fig. 2. Measured (continuous lines) and calculated (dotted lines) (a) real and (b) imaginary parts of the effective permeability, at the different magnetic states $m = 0.5, -0.1, -0.7$ configured by field cycling over the major hysteresis loop (see the inset), for the array of Ni$_{83}$Fe$_{17}$ NWs embedded in a PC membrane with packing fraction $P = 3.4\%$. The measured parts $\Re(\mu_{\text{exp}})$ and $\Im(\mu_{\text{exp}})$ and calculated parts $\Re(\mu_{\text{eff}})$ and $\Im(\mu_{\text{eff}})$ of the permeability are obtained from (7) and (8).

virtue of the dependence of the peaks' amplitude on the value of m. Since the absorption of each FMR peak is proportional to the fraction of $m_\pm$ NWs in each magnetization direction as suggested by (4)–(6), it follows that as the amplitude of one peak increases the other decreases due to the conservative feature of the number of $m_\pm$ NWs [26] via the relation $m_+ + m_- = 1$. Therefore, by setting the value of m close to the saturated state, absorption is expected to become asymmetrical and depending on whether the system is close to positive ($m = 1$) or negative ($m = -1$) saturation, each absorption beside f_{bp} is then either diminished or enhanced.

On the other hand, the behavior of a microwave filter depends on its ability to absorb microwave energy, so its characteristics can be identified directly from the insertion loss (S) expressed in dB and defined as the magnitude of the transmission factor T. Theoretically, this parameter can be obtained from the effective permeability given by (7) along with the complex propagation constant $k_z = (2\pi f/c_0)(\varepsilon_{\text{eff}}\mu_{\text{eff}})^{1/2}$, which is determined using a variational approach [28]. That is, the constant k_z is used as input parameter for the calculation of T via the expression

$$T = e^{-jk_z L} \qquad (9)$$

so that the insertion loss writes $S = -20\log_{10}|T| = 20L\Re(k_z)\log_{10} e$, which in turn allows to reproduce the absorption spectra of unsaturated arrays of bistable magnetic NWs. In the following, we discuss the microwave filter functionalities by comparing measured and calculated absorption spectra using the proposed model along with input parameters like the saturation magnetization, packing fraction, NWs length, damping factor, and the magnetic state, which are determined from FMR and AGM experiments.
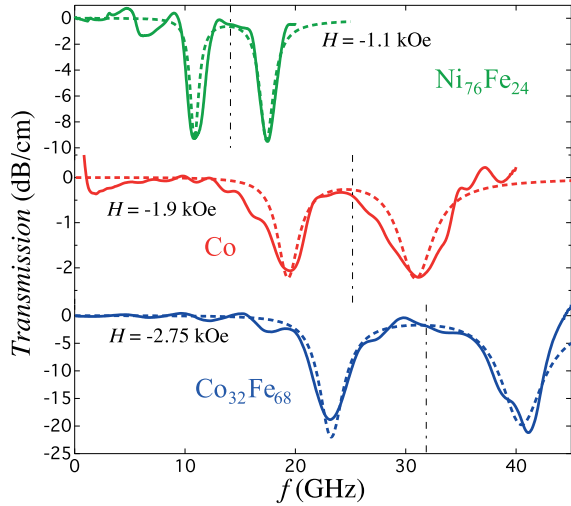
Fig. 3. Measured (continuous lines) and calculated (dashed lines) FMR spectra for an array of Co NWs in a PC membrane and arrays of NiFe and CoFe NWs in AAO membranes. Their respective local bandpass frequency (f_{bp}) (indicated by vertical dashed–dotted lines) is equal to 14.12, 25.14, and 31.86 GHz. The applied field for each array of NWs corresponds approximately to its respective coercive field.

IV. RESULTS

A. Bandpass Mode

When an array of bistable NWs is subjected to an external field such that its magnetic state is brought from saturation to an unsaturated state over the major hysteresis loop, the double FMR absorption appears by virtue of the FMR absorption of each population of $m_\pm$ NWs [26]. As mentioned above, a passband is present in the spectra at the frequency value given by (2), as a result of the frequency gap present between the absorptions for the m_+ and m_- NWs, providing the characteristics of a bandpass filter. Particularly, the optimal passband occurs when both absorptions for the $m_\pm$ NWs have the same amplitude. This is accomplished only when $m_+ = m_-$ (or $m = 0$), that is, when the return field equals the coercive field value H_c. Fig. 3 shows measured (continuous lines) and calculated (dashed lines) FMR spectra at return fields $H \approx H_c$ for an array of Co NWs in a PC membrane with $P = 3\%$ and $h_w = 0.2$ and arrays of NiFe and CoFe NWs in AAO membranes with $P = 8.5\%-10\%$ and $h_w = 0.2-0.4$. As observed, the midpoint between the two resonance frequencies $f_{m_\pm}$ (vertical dashed–dotted lines in Fig. 3) gives the minimum absorption, which indeed corresponds to the local bandpass frequency given by (2). Since f_{bp} is independent of the magnetic state m, it can be engineered using either material parameters (γM_s) or the NWs packing fraction (P). These parameters have a significant impact on the value of the out-of-band rejection ratio as observed from the larger values obtained for the NiFe and CoFe arrays of NWs in AAO porous membranes. Comparing the spectra for these arrays with that for the array of Co NWs in a PC membrane, it is clear that improved performances of the bandpass mode can be obtained for larger M_s, P, and h_w. Moreover, the effect of these parameters in the bandpass filter mode also allows to modify the value of the bandwidth Δf, as suggested
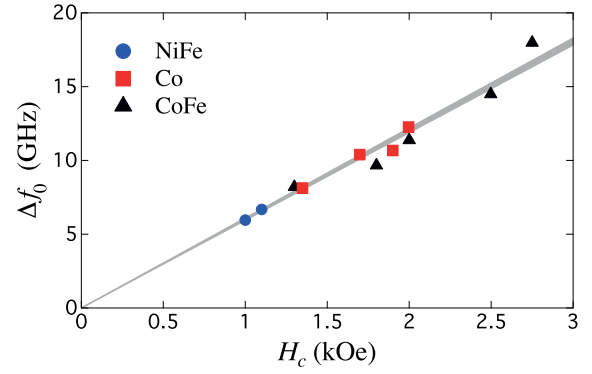
Fig. 4. Bandpass bandwidth (Δf_0) as a function of the coercive field (H_c) for the arrays of NWs of Table I, which were configured in the optimum bandpass mode with absorption peaks of equal amplitude ($m = 0$). The continuous line corresponds to the equation $\Delta f_0 = 2\gamma H_c$ and the shaded region within it represents the variation of γ due to the different materials.

by (3). Particularly, the bandpass bandwidth $\Delta f_0 = 2\gamma H_c$ given by (3) with $m = 0$ for the optimal bandpass filter, depends only on the corresponding H_c value, so the resonance frequencies at the coercive field that define the value of Δf_0 can be written as

$$f_{m_\pm}^{(H_c)} = f_{bp} \pm \gamma H_c. \tag{10}$$

Fig. 4 shows the variation of Δf_0 as a function of H_c for different arrays of NiFe, Co, and CoFe NWs, whose material parameters and packing fractions are given in Table I. As observed, the experiment is in very good agreement with the predicted dependence of Δf_0 with H_c. This shows that a bandpass filter for high-frequency performances with large Δf_0 can be engineered by choosing a magnetic material with both large M_s and H_c, as seen in Fig. 3 for the $Co_{32}Fe_{68}$ sample with $M_s = 1950$ emu/cm^3 and $|H_c| = 2.75$ kOe.

B. Bandstop Mode

One particular advantage or property of these systems is that once a given magnetic configuration is obtained for a given return field, it is possible to modulate or tune the filter bandwidth Δf by varying the applied magnetic field, as suggested by (3). Indeed, consider an FMR first-order reversal curve (FMR-FORC) as that shown by the dotted line in the inset of Fig. 5(a). These curves are obtained by measuring the dispersion relation after reversal of the magnetic field from the value H_r on the major hysteresis loop back to saturation. Fig. 5(a) shows the as-measured (symbols) and calculated (continuous lines) FMR-FORC between H_r and zero field corresponding to the dispersion relations for the m_+ (filled circles) and m_- (empty circles) NWs. As the field is lowered from H_r down to zero field, between the two filled squares shown in the inset of Fig. 5(a), each dispersion relation follows a linear dependence, provided m remains constant. A characteristic of these FMR-FORCs is that both the dispersion relations lie within the dispersion relations for the isolated NW (dotted lines) and the saturated state (dashed–dotted lines) and cross each other at a field value equal to H_{int}. This means that Δf, and as a consequence its selectivity,
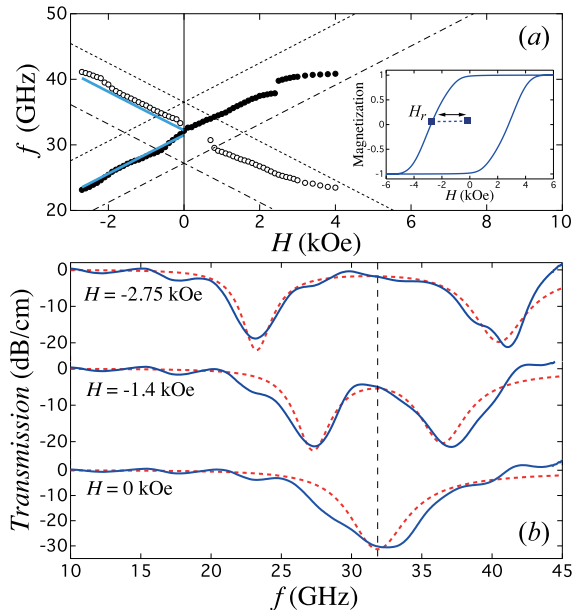
Fig. 5.   (a) FMR-FORC dispersion relation for the f_{m+} (filled circles) and f_{m-} (empty circles) frequencies measured on the array of $Co_{32}Fe_{68}$ NWs in an AAO membrane with a return field $H_r = -2.75$ kOe (see the inset), where $m = +0.07$ is stable in the range between H_r and zero field. The calculated dispersion relations (continuous lines), based on (1), lie within the dispersion relations for the isolated NW (dotted lines) and for the saturated array of NWs (dashed–dotted lines). (b) Measured (continuous lines) and calculated (dashed lines) FMR spectra over the FMR-FORC of (a) at field values of -2.75, -1.4, and 0 kOe.

can be differentially tuned with small applied field values such that it becomes very narrow and disappears at $H = H_{int}$, as predicted by (3), where both the absorption peaks superpose.

Actually, at zero field the absorption spectra contains a single peak for any magnetic configuration, which means that the bandpass filter turns into a bandstop filter. Based on the use of FMR-FORCs, the optimal operation configuration is when $m = 0$, since in this state the absorption depth of both the peaks is identical and the bandwidth of the bandpass can be tuned with an applied field as suggested by (1) and (3). Fig. 5(b) shows absorption spectra configured at $m = +0.07$, that is, recorded over the reversible part of the FMR-FORC at applied fields $H_r = H_c \approx -2.75$ kOe, $H = -1.4$ kOe, and zero field. The corresponding resonance frequencies $f_{m\pm}$ are obtained using (10) for $H_r = -2.75$ kOe and using H instead of H_c for the other two field values. As long as the magnetic state of the system remains stable along an FMR-FORC, the system can perform other functions. For example, the reversible passing from the bandpass to the bandstop mode as the field is lowered (increased) between the return and zero fields (as seen by the two-headed arrow between the two filled squares in the inset). In this case, the zero field bandstop frequency corresponds to the configuration-dependent zero field FMR frequency $f_{H=0}^{(m)} = 2\pi M_s \gamma [1 - 3P(1 + |m|)/2]$ reported in [27]. This expression is such that $f_{H=0}^{(m)} = f_{bp}$ for $m = 0$, which corresponds to the maximum attainable zero field resonance frequency value when the populations

of m_+ and m_- NWs are equal [27]. Then the difference $f_{bp} - f_{H=0}^{(m)}$ is equal to $3\pi M_s P \gamma |m| = \gamma |H_{int}|$, which is maximum when m tends to ± 1. Therefore, $f_{H=0}^{(m)}$ can be tuned by configuring the magnetic state of the filter and its range of tunability depends directly on H_{int}. This advantageously compares with on-wafer bandstop magnetic filters for which the zero field bandstop frequency is fixed and depends only on material parameters [3], [30]. Finally, it is worth mentioning that multifunctional microwave filters may be engineered using multiferroic nanostructured composites in which their magnetic and microwave properties can be electrically controlled, instead of using external fields, by virtue of the mechanical coupling between the magnetostrictive and piezoelectric phases [31], [32].

V. CONCLUSION

We have proposed a bifunction and low-field cycling microwave filter prototype based on arrays of bistable NWs, which takes advantage of the double FMR effect. Our module is capable of working as a bandpass filter in unsaturated states where the double FMR absorption takes place and as a bandstop filter when the system is at remanence and presents a single absorption. By appropriate field cycling, one can reversibly change between these two different working modes. In addition, the configuration-dependent absorption characteristics of the present bifunction microwave filter are well reproduced using a proposed model that is based on a bistable macrospin formalism for the permeability of the array of NWs. The use of different porous membranes as host templates for the NWs permitted to show that the length, packing fraction, and saturation magnetization of the NWs are crucial parameters to significantly enhance the out-of-band rejection ratio of the proposed filter. It is important to emphasize that the concept proposed in this paper is conceivable with different noncylindrical geometries as long as bistability is assured, as for example, systems such as bit patterned media developed for perpendicular magnetic recording with enough magnetic material to ensure well-detectable FMR absorption. Simulations using expression (9) predicting the transmission can be used as a further step to optimize the filtering performances of the device.

REFERENCES

[1] M. Golio and J. Golio, *The RF and Microwave Handbook: RF and Microwave Circuits, Measurements, and Modeling*, 2nd ed. Boca Raton, FL, USA: CRC Press, 2008.
[2] V. G. Harris, "Modern microwave ferrites," *IEEE Trans. Magn.*, vol. 48, no. 3, pp. 1075–1104, Mar. 2012.
[3] R. E. Camley *et al.*, "High-frequency signal processing using magnetic layered structures," *J. Magn. Magn. Mater.*, vol. 321, no. 14, pp. 2048–2054, Jul. 2009.
[4] J. Zhang, J. Zhao, R. Peng, J. Li, R. Zhang, and M. Wang, "Tunable microwave filters and phase shifters based on ferromagnetic/dielectric multilayer waveguides," *Jpn. J. Appl. Phys.*, vol. 49, no. 3R, Mar. 2010, Art. no. 033004.
[5] N. R. Anderson and R. E. Camley, "Multilayer magnetic waveguides: Optimizing nonreciprocal propagation in the 50–70 GHz range," *J. Appl. Phys.*, vol. 116, Jul. 2014, Art. no. 023903.
[6] B. K. Kuanr, V. Veerakumar, R. Marson, S. R. Mishra, R. E. Camley, and Z. Celinski, "Nonreciprocal microwave devices based on magnetic nanowires," *Appl. Phys. Lett.*, vol. 94, no. 20, May 2009, Art. no. 202505.

[7] V. Van Kerckhoven, L. Piraux, and I. Huynen, "Substrate integrated waveguide isolator based on ferromagnetic nanowires in porous alumina template," *Appl. Phys. Lett.*, vol. 105, no. 18, Nov. 2014, Art. no. 183107.

[8] M. Darques, J. De La Torre Medina, L. Piraux, L. Cagnon, and I. Huynen, "Microwave circulator based on ferromagnetic nanowires in an alumina template," *Nanotechnology*, vol. 21, no. 14, Mar. 2010, Art. no. 145208.

[9] G. Hamoir, L. Piraux, and I. Huynen, "Control of microwave circulation using unbiased ferromagnetic nanowires arrays," *IEEE Trans. Magn.*, vol. 49, no. 7, pp. 4261–4264, Jul. 2013.

[10] C. E. Carreón-González, J. De La Torre Medina, A. Encinas, and L. Piraux, "Electrodeposition growth of nanowire arrays with height gradient profiles for microwave device applications," *Nano Lett.*, vol. 11, no. 5, pp. 2023–2027, Apr. 2011.

[11] G. Hamoir, J. De La Torre Medina, L. Piraux, and I. Huynen, "Self-biased nonreciprocal microstrip phase shifter on magnetic nanowired substrate suitable for gyrator applications," *IEEE Trans. Microw. Theory Techn.*, vol. 60, no. 7, pp. 2152–2157, Jul. 2012.

[12] M. Sharma, B. K. Kuanr, M. Sharma, and A. Basu, "Tunable EMI noise suppressor based on Ni nanowire arrays," *Phys. B, Condens. Matter*, vol. 448, pp. 316–319, Sep. 2014.

[13] A. Encinas, L. Vila, M. Darques, J.-M. George, and L. Piraux, "Configurable multiband microwave absorption states prepared by field cycling in arrays of magnetic nanowires," *Nanotechnology*, vol. 18, no. 6, Jan. 2007, Art. no. 065705.

[14] M. Zhang, Y. Nozaki, and K. Matsuyama, "Reconfigurable ferromagnetic resonance properties in nanostructured multilayers," *J. Appl. Phys.*, vol. 99, no. 8, Apr. 2006, Art. no. 08G307.

[15] Y. Nozaki, K. Tateishi, S.-I. Taharazako, S. Yoshimura, and K. Matsuyama, "Bistable control of ferromagnetic resonance frequencies in ferromagnetic trilayered dots," *J. Appl. Phys.*, vol. 105, no. 1, Jan. 2009, Art. no. 013911.

[16] B. K. Kuanr, R. Marson, S. R. Mishra, A. V. Kuanr, R. E. Camley, and Z. Celinski, "Gigahertz frequency tunable noise suppressor using nickel nanorod arrays and permalloy films," *J. Appl. Phys.*, vol. 105, no. 7, Mar. 2009, Art. no. 07A520.

[17] M. Sharma, B. K. Kuanr, M. Sharma, and A. Basu, "New opportunities in microwave electronics with ferromagnetic nanowires," *J. Appl. Phys.*, vol. 115, no. 17, Feb. 2014, Art. no. 17A518.

[18] J. Ni and J. Hong, "Varactor-tuned microstrip bandpass filters with different passband characteristics," *IET Microw. Antennas Propag.*, vol. 8, no. 6, pp. 415–422, Apr. 2014.

[19] L. Athukorala and D. Budimir, "Frequency tunable microstrip resonators and filters," in *Proc. 39th Eur. Microw. Conf. (EuMC)*, Sep./Oct. 2009, pp. 1239–1242.

[20] X. Luo, S. Sun, and R. B. Staszewski, "Tunable bandpass filter with two adjustable transmission poles and compensable coupling," *IEEE Trans. Microw. Theory Techn.*, vol. 62, no. 9, pp. 2003–2012, Sep. 2014.

[21] J. Hong, J. Ni, F. Cervera, and L. Hepburn, "Recent advances in microwave planar filter technology," *IEICE Trans. Electron.*, vol. E98-C, no. 7, pp. 598–607, Jul. 2015.

[22] H. Zhu and A. Abbosh, "Compact tunable bandpass filter with wide tuning range of centre frequency and bandwidth using coupled lines and short-ended stubs," *IET Microw. Antennas Propag.*, vol. 10, no. 8, pp. 863–870, Feb. 2016.

[23] Y. Zhu, G. Qiu, K. H. Chi, B. B. T. Wang, and C. S. Tsai, "A tunable X-band band-pass filter module using YIG/GGG layer on RT/duroid substrate," *IEEE Trans. Magn.*, vol. 45, no. 10, pp. 4195–4198, Oct. 2009.

[24] Y. Zhu, G. Qiu, K. H. Chi, B. B. T. Wang, and C. S. Tsai, "A compact X-band tunable bandpass filter module using a pair of microstrip composite bandpass filters in cascade," *IEEE Trans. Magn.*, vol. 46, no. 6, pp. 1424–1427, Jun. 2010.

[25] M. Darques, A. Encinas, L. Vila, and L. Piraux, "Controlled changes in the microstructure and magnetic anisotropy in arrays of electrodeposited Co nanowires induced by the solution pH," *J. Phys. D, Appl. Phys.*, vol. 37, no. 10, pp. 1411–1416, Apr. 2004.

[26] J. De la Torre Medina, L. Piraux, J. M. O. Govea, and A. Encinas, "Double ferromagnetic resonance and configuration-dependent dipolar coupling in unsaturated arrays of bistable magnetic nanowires," *Phys. Rev. B*, vol. 81, no. 14, Apr. 2010, Art. no. 144411.

[27] J. De la Torre Medina, L. Piraux, and A. Encinas, "Tunable zero field ferromagnetic resonance in arrays of bistable magnetic nanowires," *Appl. Phys. Lett.*, vol. 96, no. 4, Jan. 2010, Art. no. 042504.

[28] J. Spiegel and I. Huynen, "A variational approach for propagation in ferromagnetic nanowired composite," *J. Comput. Theor. Nanosci.*, vol. 6, no. 9, pp. 2001–2008, Sep. 2009.

[29] J. Spiegel, J. De La Torre, M. Darques, L. Piraux, and I. Huynen, "Permittivity model for ferromagnetic nanowired substrates," *IEEE Microw. Wireless Compon. Lett.*, vol. 17, no. 7, pp. 492–494, Jul. 2007.

[30] B. K. Kuanr, Z. Celinski, and R. E. Camley, "Tunable high-frequency band-stop magnetic filters," *Appl. Phys. Lett.*, vol. 83, no. 19, pp. 3969–3971, Nov. 2003.

[31] L. Piraux *et al.*, "Template approach for novel magnetic–ferroelectric nanocomposites," *Appl. Phys. Exp.*, vol. 4, no. 11, Oct. 2011, Art. no. 115001.

[32] F. Rasoanoavy *et al.*, "Magnetodielectric effect in trilayered $Co_{65}Fe_{35}B_{20}/PVDF/Co_{65}Fe_{35}B_{20}$ composite materials. Prediction and measurement for tunable microwave applications," *J. Appl. Phys.*, vol. 107, no. 9, May 2010, Art. no. 09E313.

Rossana Ramírez-Villegas, photograph and biography not available at the time of publication.

Isabelle Huynen (S'87–M'89–SM'06), photograph and biography not available at the time of publication.

Luc Piraux, photograph and biography not available at the time of publication.

Armando Encinas, photograph and biography not available at the time of publication.

Joaquin De La Torre Medina, photograph and biography not available at the time of publication.